Attitude Control Experiments of Cubic Rover on Low‐Gravity Testbed[①]

ZENG Xiangyuan[1*], JIANG Bowen[1], HUSSAIN Muhammad Talha[1],

JIANG Jianxun[2], YANG Runyi[1]

1. School of Automation, Beijing Institute of Technology, Beijing 100081, P. R. China；

2. System Engineering Research Institute, China State Shipbuilding Corporation, Beijing 100094, P. R. China

Abstract: In‐situ exploration of asteroid surfaces is of great scientific significance. Internally actuated rovers have been released to asteroid surfaces but without enough controllability. To investigate the attitude control characteristics of the cubic rover for asteroid surface exploration, a series of experiments are carried out using the self‐designed rover and the low‐gravity testbed. The experiments focus on two major themes：The minimum flywheel speed for cubic rover to produce a walking motion in different conditions, and the relationship between the rover's rotation angle and the flywheel speed in twisting motion. The rover's dynamical descriptions of the walking and twisting motions are first derived. The features and design of the low‐gravity testbed are then summarized, including its dynamics, setup, and validation. A detailed comparison between the dynamic model and the experimental results is presented, which provides a basic reference of the cubic rover's attitude control in low‐gravity environments.

Key words: cubic rover；low‐gravity testbed；walking motion；twisting motion；planetary exploration

CLC number: V412.4   **Document code:** A   **Article ID:** 1005‐1120(2022)02‐0143‐09

0 Introduction

There is a new surge of interest in exploring small celestial bodies such as asteroids and near‐Earth objects in recent years due to their unique exploration value[1]. The recent planetary science decadal survey has prioritized three cross‐cutting themes for planetary exploration：The characterization of the early solar system history, the search for planetary habitats, and an improved understanding about the nature of planetary processes[2]. On that account, the controlled mobility in low‐gravity ($10^{-1}g$—$10^{-3}g$) and micro‐gravity ($10^{-3}g$—$10^{-6}g$) environments has been recognized as crucial to space research centers around the world for further technological development, and is also one of the major challenges faced by planetary rovers today. It is mainly challenging due to the un‐structured terrains and the low surface friction[3-4]. A multitude of mobility approaches for planetary rovers have been proposed, including mobility via thrusters, wheels, legs, and hopping. Thruster‐type rovers consume large quantity of energy which makes them unsuitable for long‐haul planetary exploration. The wheeled rovers need a certain amount of traction to navigate on a rocky terrain. However, the rover can lose contact with the surface and exceed the escape velocity in a low‐gravity environment due to little traction. Legged rovers heavily rely on anchoring devices, which has complex mechanical structure and makes them highly dependent on the surface characteristics. For instance, the failure of Philae's surface landing mission clearly illustrates the technical challenges of surface anchoring on small celestial

bodies. On the other hand, hopping rovers exploit the low-gravity environment and better adapt to the weak and irregular gravitational field on the surface of small celestial bodies[5]. Moreover, the take-off process of hopping rovers is more effective in overcoming obstacles and has good adaptability to complex terrain.

Due to the practicality of mobility via hopping, numerous hopping rovers and their mobility characteristics have been investigated in the last decade. In 2012, Zurich polytechnic developed an internally actuated rover called Cubli[6]. Cubli has three mutually orthogonal flywheels that are actuated by three DC brushless motors and braked instantly to make the rover jump up and balance on a corner. In the next year, the same team further analyzed Cubli's orientation in a corner balancing experiment[7]. In 2013, Romanishin et al. developed a cubic rover named M-Blocks with a side length of only 25 mm[8]. M-blocks can change the geometry freely by self-assembling among multiple cubes to adapt to unstructured environments. However, it is difficult for M-blocks to adjust the attitude accurately. In 2014, Koenig et al. analyzed the dynamical behavior of hopping rover including hopping initiation and instrument pointing aspects in microgravity environment[9]. In 2016, Hockman et al. designed a cubic rover with three-dimensional flywheels and a gravity-offloading system that simulates a low-gravity environment[10]. They conducted experiments to verify the hopping and twisting dynamics of the rover. However, they did not conduct experiments to investigate the walking and twisting motions in low-gravity environment. In 2022, Wang et al. designed a spherical robot that can exhibit rolling and jumping motions[11]. The motion characteristics of the robot were tested by numerical simulation under different gravity levels and concluded that the robot shows better mobility in low-gravity environment.

In general, the research on attitude control characteristics and the ground tests of the cubic rover in a low-gravity environment are still limited. In particular, the walking and twisting motions have not been thoroughly investigated in a low-gravity environment. In order to study the wide spectrum of cubic rover's attitude control, a low-gravity testbed is proposed in this paper to conduct the ground-based experiments. Section 1 analyzes the cubic rover's dynamic models of the attitude adjustment motion referred to as walking and twisting. In Section 2, the dynamics and development of a low-gravity testbed are illustrated. In Section 3, the procedures and results of the mobility experiments in various conditions are summarized and discussed. Section 4 is the conclusion part of this paper.

1 Dynamics of Cubic Rover

The cubic rover is generally equipped with three orthogonal flywheels which are accelerated by motors and stopped by mechanical brakes. It can theoretically demonstrate three types of primitive movements: hopping, walking, and twisting. Hopping motion requires massive torque and instantaneous braking to make the rover hop in one direction. Walking motion requires less torque, where the cubic rover's pivot point does not lose ground contact throughout the process. Twisting motion requires minimal torque from the top/bottom flywheel, where the cubic rover exhibits planar rotation.

In this study, the self-designed rover is equipped with DC motors that power the flywheels, 20 kg digital servos that power the mechanical brakes, encoders that read the flywheels' speed and a STM32F103 microcontroller that administers all the actuators and sensors. The rover and its gimbal-frame are shown in Fig.1.

The focus of this section is the attitude control of the rover by analyzing the dynamics of walking and twisting motions.
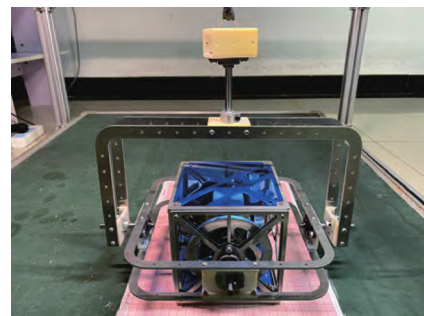

Fig.1   Cubic rover and its gimbal-frame

1.1 Walking dynamics

The purpose of formulating the walking dynamics is to obtain the most energy efficient setting for the rover in different conditions. When the internal-flywheel accelerates to the target speed, the brakes are applied instantly which transfers the kinetic energy of the flywheel to the rover, thus producing walking motion as shown in Fig.2.
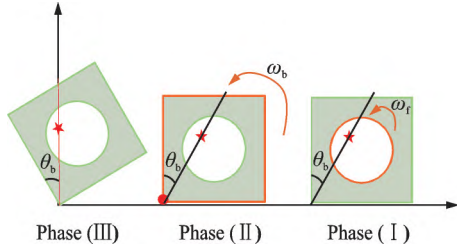

Fig.2   Illustration of the walking motion

In order to determine the flywheel's speed limit (the minimum speed for the rover to produce walking motion) in a low-gravity environment, the angular velocity of the rover is defined as ω_b, whereas ω_f is the anglular volocity of the flywheel. When the flywheel reaches the target speed in Phase (I), the brakes are applied, resulting in the momentum gain of the rover to produce inverted pendulum motion as shown in Phase (II). According to Ref.[6], the braking process is assumed as a perfect inelastic collision, i.e., a zero coefficient of restitution. Therefore, the equation for transition from Phase (I) to Phase (II) can be written as

$$I_f\omega_f = \left(I_f + I_b + m_f l_f^2\right)\omega_b \tag{1}$$

where friction and energy loss are not considered; I_f is the rotational inertia of the flywheel; I_b the rotational inertia of the rover without the flywheel; m_f the mass of the flywheel; and l_f the length between the central point and the pivot point. To simplify the expression of system's rotational inertia in walking motion, a new variable I_S is introduced which is equal to $I_f + I_b + m_f l_f^2$. The energy transfer from the rest position in Phase (II) to the unilateral equilibrium state in Phase (III) is

$$\frac{1}{2}I_S\omega_b^2 = \left[m_f l_f\left(1 - \cos\left(\frac{\pi}{4}\right)\right) + m_b l_b\left(1 - \right.\right.$$

$$\left.\left.\cos\theta_b\right]g \tag{2}$$

The flywheel's speed limit $\omega_{f,min}$ can be obtained by combining Eq.(1) and Eq.(2).

$$\omega_{f,min} = $$

$$\sqrt{\frac{2I_S}{I_f^2}\left[m_f l_f\left(1 - \cos\left(\frac{\pi}{4}\right)\right) + m_b l_b\left(1 - \cos\theta_b\right)\right]g} = $$

$$\sqrt{\frac{2}{\eta I_f}\left[m_f l_f\left(1 - \cos\left(\frac{\pi}{4}\right)\right) + m_b l_b\left(1 - \cos\theta_b\right)\right]g} \tag{3}$$

1.2 Twisting dynamics

The adjustment of onboard sensors' orientation and cubic rover's position requires precise control of the twisting motion. In this section, the dynamics of twisting motion is investigated to determine the rotation angle by variating flywheel's speed. The illustration of twisting motion is shown in Fig.3.
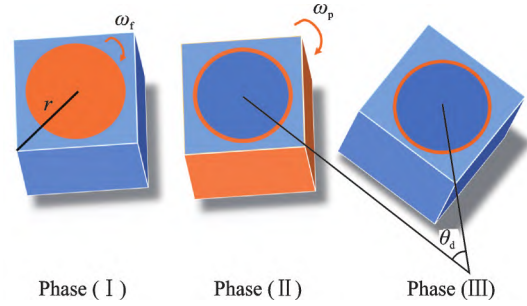

Fig.3   Illustration of the twisting motion

To simplify the analysis, the rover's mass distribution is assumed to be uniform with its center of mass coinciding with its central point. The support force is N_d; the coefficient of kinetic friction between the ground and the cubic rover is μ_d; the rotational inertia of the system around the central axis is I_p; the initial angular velocity of the flywheel is ω_p; the distance between the central axis of the rover and the pivot point is r; and the final rotation angle is θ_d. As the braking of flywheel is instant, it does not cause momentum buildup and immediately transfers kinetic energy to the rover. The equation for the conservation of angular momentum from the moment flywheel reaches maximum speed in Phase (I) to the moment rover gains angular momentum in Phase (II) can be shown as follows

$$I_f\omega_f = I_p\omega_p \tag{4}$$

The energy transfer equation from the moment rover starts twisting in Phase (II) to the moment rover stops twisting in Phase (III) is

$$\frac{1}{2} I_{\mathrm{p}} \omega_{\mathrm{p}}^2 = \mu N_{\mathrm{d}} r \theta_{\mathrm{d}} \qquad (5)$$

By combining Eq.(4) and Eq.(5), the relationship between flywheel speed and the rotation angle can be obtained as follows

$$\omega_{\mathrm{f}} = \frac{I_{\mathrm{p}}}{I_{\mathrm{f}}} \sqrt{\frac{2\mu_{\mathrm{d}} N_{\mathrm{d}} r \theta_{\mathrm{d}}}{I_{\mathrm{p}}}} \qquad (6)$$

Finally, converting the speed unit to r/min yields

$$n = \frac{2\pi}{60} \frac{I_{\mathrm{p}}}{I_{\mathrm{f}}} \sqrt{\frac{2\mu_{\mathrm{d}} N_{\mathrm{d}} r \theta_{\mathrm{d}}}{I_{\mathrm{p}}}} \qquad (7)$$

2 Low-Gravity Testbed

The validation of rover's dynamics based on ground tests in low-gravity environment is significant for mission design. It is immensely challenging to simulate a microgravity/low-gravity environment on Earth. The zero-g drop tower facilities and zero-g planes offer effective microgravity but expensive, and they cannot be used for recurrent experiments because of the transience of microgravity periods. The microgravity testbed developed by Hockman et al.[10] in 2016 actively generates a vertical counterbalance force which requires high power, sophisticated control, and is an expensive system overall. For the sake of iterative validation and improvement of the cubic rover, a cost-efficient testbed is proposed in this study. It is easy to set up, requires minimal power, and offers sufficient periods of low-gravity. This section presents the dynamic model, setup, and validation of our low-gravity testbed.

2.1 Dynamic modeling

The low-gravity testbed is based on the Atwood principle which is configured as a gravity offloading system. The modeling parameters are mentioned in Table 1.

Fig.4(a) shows the simulated gravity force on the cubic rover suspended over two pulleys with a counterweight. Fig.4(b) illustrates the low-gravity force acting on the rover on a slope.

In the moments before its motion, the rover is resting on the low-gravity body's surface. One can easily obtain that

Table 1   Parameters of the low-gravity testbed modeling

Parameter	Definition
M	Total mass of the cubic rover
m_{e}	Mass of counterweight
g	Gravitational acceleration
g_{a}	Gravitational acceleration of low-gravity body
θ	Surface inclination
N_{e}	Support force on the testbed
N_{a}	Support force on the surface
f_{s1}	Static friction on the surface
f_{s2}	Static friction on the testbed
T	Tensile force from wire
μ_{s}	Static friction coefficient

(a) Rover on the low-gravity testbed   (b) Rover on the celestial bodies
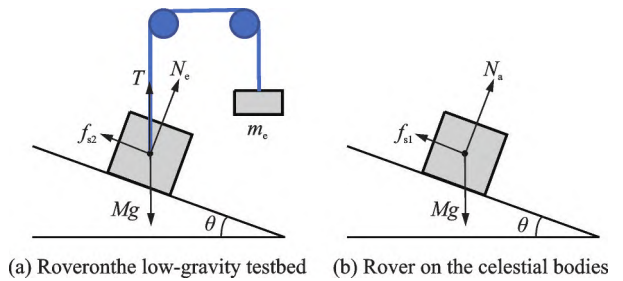
Fig.4   Rover resting on the surface

$$\begin{cases} Mg_{\mathrm{a}} \sin\theta - f_{\mathrm{s1}} = 0 \\ N_{\mathrm{a}} - Mg_{\mathrm{a}} \cos\theta = 0 \\ f_{\mathrm{s1}} = \mu_{\mathrm{s}} N_{\mathrm{a}} \end{cases} \qquad (8)$$

When simulating this pose on our low-gravity testbed, it can be described as

$$\begin{cases} Mg \cos\theta - T\cos\theta - N_{\mathrm{e}} = 0 \\ Mg \sin\theta - T\sin\theta - f_{\mathrm{s2}} = 0 \\ T = m_{\mathrm{e}} g \\ f_{\mathrm{s2}} = \mu_{\mathrm{s}} N_{\mathrm{e}} \end{cases} \qquad (9)$$

Assuming that N_{e} is equivalent to N_{a} and combining Eq.(8) and Eq.(9), one can obtain the simulated gravitational acceleration of the low-gravity body, shown as

$$g_{\mathrm{a}} = \left(1 - \frac{m_{\mathrm{e}}}{M}\right) g \qquad (10)$$

When the rover loses contact with the surface and is in the air, the contact forces are zero where only the gravitational attraction is applied. Fig.5(a) shows the rover on the low-gravity testbed without any contact with the surface. The equation for the system is

$$\begin{cases} Mg - T = Mg \\ T - m_e g = m_e g \end{cases} \quad (11)$$

Fig.5(b) shows the rover midair on the low-gravity body's surface where the rover is only affected by the gravitational acceleration of low-gravity body Mg_a.
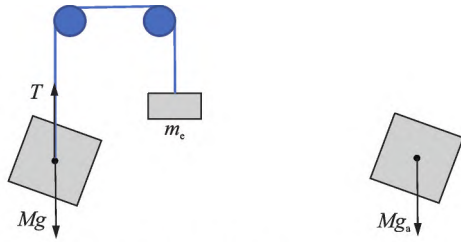
(a) Rover on the low-gravity testbed   (b) Rover on the celestial bodies

Fig.5   Rover in the air

Assuming that the rover is undergoing the same accumulated forces yield the expression for the simulated gravitational acceleration g_s that

$$g_s = \frac{M - m_e}{M + m_e} g \quad (12)$$

2.2   Testbed setup

The testbed is constructed with sturdy aluminum square rods to minimize the vibrational effect. Its size is 1 m ×1 m ×1 m in the XYZ-plane. The three-axis rotational motion of the cubic rover is achieved by mounting it within a lightweight gimbal frame. The gimbal-mounted rover is secured through its center of mass by a shaft and a pair of bearings so that it could rotate freely. The experimental environment and the testbed setup are shown in Fig.6 and Fig.7, respectively.

One high-tensile steel wire is connected to the bearings, looped over two pulleys, and connected
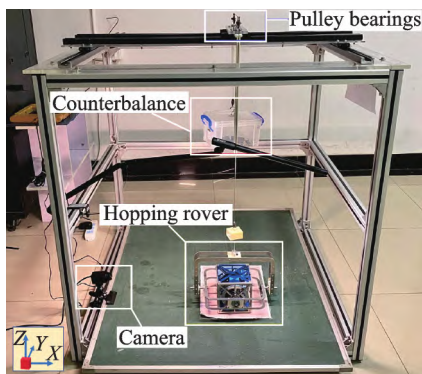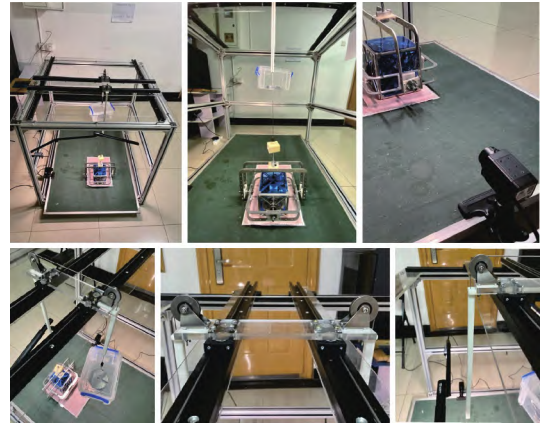

Fig.6   Overview of experimental environment

Fig.7   Testbed setup

to a counterweight suspended on the other side. The pulleys are mounted on frictionless sliders that allowed movement along X-axis and Y-axis. With the counterweight offsetting most of the rover's mass, experiments were performed on a wooden surface. The surface inclination is adjusted manually and calibrated using MPU6050. Using the current testbed, we can simulate the gravity level of $10^{-2}g$ which is slightly higher than the Phobos' gravity. The rover's pose is tracked using an external video camera for capturing motion state transitions. The experimental procedure includes preparations such as aligning the pulleys to minimize friction, and then allowing the rover to come to rest on the surface.

2.3   Validation of testbed

2.3.1   Precision

The precision of the testbed demonstrates how close the simulated gravity level is to the ideal gravity level. The formula to calculate the precision is given below

$$\xi = 1 - \frac{|N - (M - m_e)|}{M - m_e} \quad (13)$$

where $M - m_e$ represents the expected outcome of the gravity offloading system and the support force N represents the actual outcome of the gravity offloading system.

A multitude of experiments were conducted where we changed the counterweight m_e and measured the support force N on the surface to obtain the precision of our testbed. The results are summarized in Fig.8. The ideal g coefficient g_a is the multiples of the gravitational constant, derived from
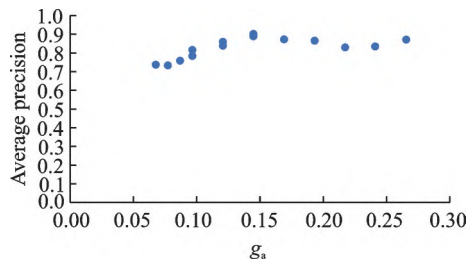
Fig.8 Analysis of precision

Eq.(10) which is compared with the average preci-
sion. As shown in the graph, the testbed exhibits a
good trend of average precision along the increasing
values of ideal g.

2.3.2 Mobility of testbed

A series of experiments were performed on var-
ious inclinations under different gravity levels to vali-
date the testbed's versatility. The testbed can simu-
late a variety of environmental conditions: Surface
inclination ranging from $-4°$ to $4.07°$ and gravity
level ranging from $0.036g$ to $1g$.

Fig.9 illustrates the viability of testbed where a
complete walking motion of the rover is shown. The
rover performed this walking motion on a flat sur-
face under the simulated gravity level of $0.049g$,
with the flywheel speed set to 3 900 r/min which is
approximately the lowest speed parameter that
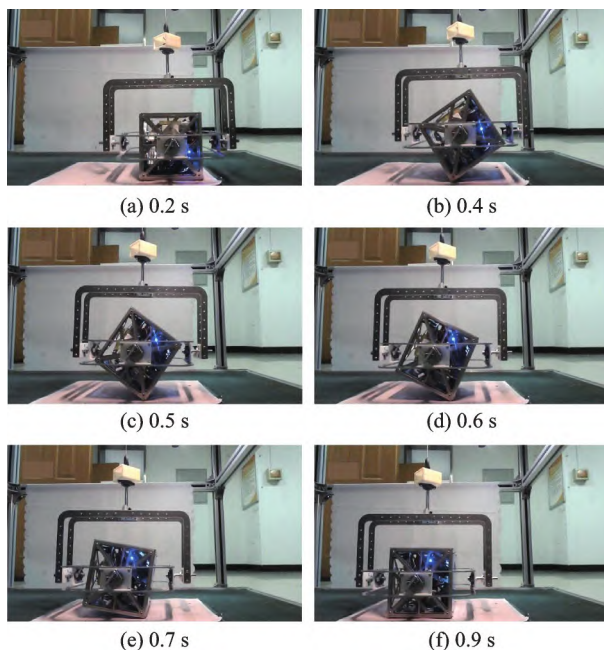makes the rover produce a walking motion.

(a) 0.2 s (b) 0.4 s (c) 0.5 s (d) 0.6 s (e) 0.7 s (f) 0.9 s

Fig.9 Different mobility states of cubic rover with respect
to time

3 Ground Experiments

In order to verify the consistency and accuracy
of theoretical formulation, ground tests were car-
ried out to analyze the flywheel's speed limit un-
der different gravity levels as well as the relation-
ship between rover's rotation angle and flywheel
speed.

3.1 Speed limit analysis of walking motion un-
der different gravity levels

The purpose of this experiment is to obtain the
relationship between different gravity levels and fly-
wheel's speed limit. The experiment is designed as
follows: (1) The rover is placed in the center of the
testbed and powered on; (2) the lowest flywheel
speed that causes the rover to rotate, support force
on the surface, mass of the counterweight, and sur-
face inclination are recorded; (3) mass of the coun-
terweight and surface inclination is changed after
each set of the experiment. In order to minimize the
external effect and human interference on the data,
each set of experiments was conducted five times as
preliminary investigation. The values of the relevant
parameters are shown in Table 2. The representa-
tive experiment among these results can be referred
to Fig.9.

Table 2 Parameters of the low-gravity testbed modeling

Parameter	Value
l_b/m	9.2×10^{-2}
l_f/m	9.05×10^{-2}
g/(m·s^{-2})	9.812
m_b/kg	1.990
m_f/kg	8.03×10^{-2}
P/kW	2×10^{-2}
θ_b/rad	1.36
I_b/(kg·m^2)	0.031
I_f/(kg·m^2)	0.18×10^{-3}

The relationship between the experimental and
theoretical results of flywheel's speed limit under
different gravity levels is illustrated in Fig.10. In the
graph, the horizontal axis essentially represents
gravity levels simulated by the low-gravity testbed
which can be obtained from the following equation as

$$a = \frac{N}{M} \quad (14)$$

where a is the expression that yields multiples of the gravitational constant, and M the total mass of the rover. The vertical axis represents the speed limit of the flywheel which can be obtained from Eq.(6). The blue line depicts the prediction model calculated by Eq.(3). The upper and lower dashed lines are boundaries of the model obtained by adjusting system parameters.
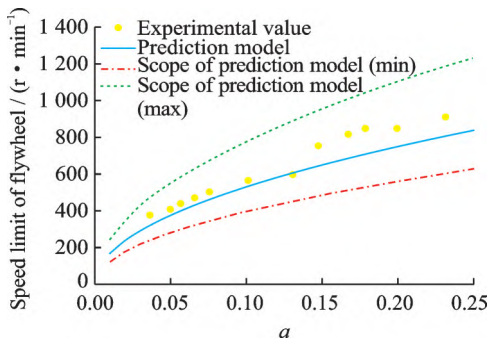

Fig.10   Relationship between g and speed limit

It can be seen from Fig.10 that the prediction model (blue line) and the experimental data (yellow dots) both lie within the model's boundaries (two dashed lines). The experimental data are consistent with the trend of the theoretical model but they are slightly higher than the theoretical model, which can be explained by the frictional loss generated by the suspension wire and sliders on the low-gravity testbed. Hence, the graph depicts that a larger speed limit is required for the cubic rover to produce a walking motion. The minor deviations in the results could be caused by the measurement error and the speed constraint which is the speed change in the increments of 300 r/min.

3.2   Rotation angle analysis of twisting motion

In order to analyze the twisting motion of the cubic rover, a series of experiments were conducted under the gravity levels of $0.076g$. We recorded the flywheel speed, the initial and the final angular position of the rover, and used the difference between these two positions as the rotation angle. Each set of experiments was performed five times to minimize errors and interferences. The results were compared with Eq.(7) to verify the accuracy. Table 3 lists the relevant parameter values.

Table 3   Parameters of the twisting experiment

Parameter	Value
r / m	8.2×10^{-2}
μ_d	0.03
$I_p/(kg \cdot m^2)$	5.8×10^{-3}
$I_f/(kg \cdot m^2)$	2×10^{-4}

Fig.11 shows the results of rotation angle exhibited by the cubic rover in low-gravity. In the figure, x-axis represents the flywheel speed and y-axis represents the rotation angle. The two dashed lines are the boundaries of the prediction model calculated by Eq.(7).
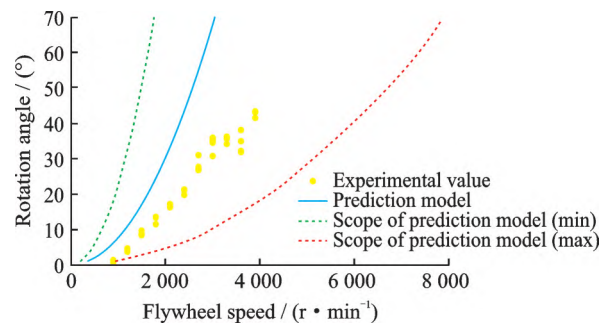

Fig.11   Relationship between flywheel speed and rotation angle

The results show that the experimental data (yellow dots) and the prediction model (blue line) are within the boundaries. Moreover, the trend of the experimental data is mainly in accordance with the prediction model.

The divergence between the prediction model and the experimental data is explained by the video sequence in Fig.12. In the experiment, the flywheel speed is set to 3 000 r/min. Figs.12(a—c) display the first half of the twisting motion, where acceleration of the flywheel creates the rotational torque greater than the torque of static ground friction. Henceforth, the rover rotates in the opposite direction exhibiting reverse motion. Figs.12(d—f) display the latter half of the motion, where the flywheel halts and the rover rotates towards the target direction and stops at a much smaller angle than expected. Therefore, the sum of the rotation angles during the twisting process (prediction model) is much larger than the angular difference between the initial and the final positions (experimental data).
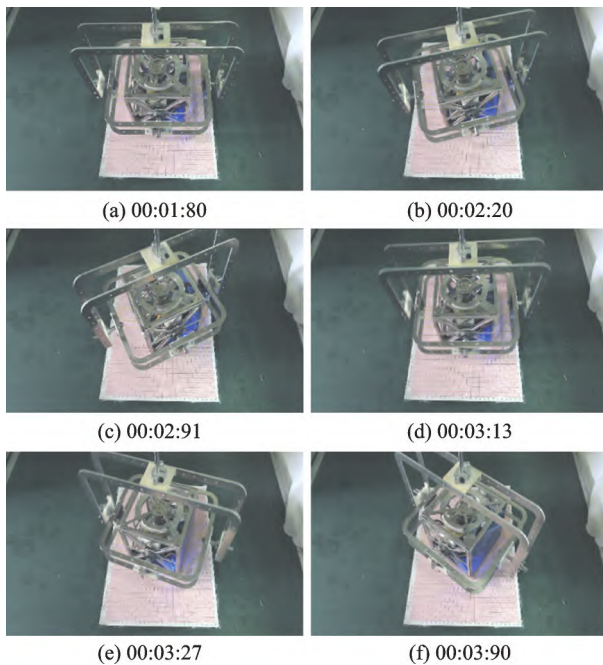
(a) 00:01:80   (b) 00:02:20

(c) 00:02:91   (d) 00:03:13

(e) 00:03:27   (f) 00:03:90

Fig.12 Different mobility states of rover during walking motion

3. 3   Discussion

As shown from the results of ground experiments, the trend of experimental data demonstrates strong consistency with the prediction model. However, there are a few limitations that leave multiple important extensions open for further research[12-13]. First, the friction in the suspension wire and the sliders caused deviances in the results of walking experiment. Ergo, we plan to incorporate an active-feedback tracking system in the testbed that uses actuators and sensors to minimize the frictional loss. Second, the reverse motion caused divergence in the results of twisting experiment which can be eliminated by reducing the acceleration of the flywheel. Third, the terrain of small celestial bodies has irregular topography, whereas the dynamic model and the testbed setup only allows experimentation on a plane surface. Hence, we plan to insert more realistic contact models for interactions with loose, granular media typically found on the surfaces of small celestial bodies. Finally, the gravity simulated by the current testbed reaches the level of $10^{-2}g$ that hinders further mobility experimentation. Therefore, we plan to emulate effective gravity levels on the order of $10^{-3}g$ that allows for full six-DoF motion with minimal exogenous dynamic interference.

4   Conclusions

This paper presents the attitude control experimentations with a cubic rover on the low-gravity testbed. The cubic rover dynamics of the walking and twisting motion are briefly summarized. The dynamics, setup, and validation of the low-gravity testbed are then illustrated. Two major experiments are performed referred to as "speed limit analysis of walking motion under different gravity levels" and "rotation angle analysis of twisting motion". In the first experiment, the results present the most energy efficient settings for the rover and show that the flywheel speed limit falls within the boundaries of prediction model under different gravity levels. In the second experiment, the rover's rotation angles mainly follow the trend of the prediction model. However, a deviation between the prediction model and the experimental data is noticed, which is caused by the rover's reverse motion. These experimental results provide significant insights into the attitude control of the cubic rover in low-gravity environments.

References

[1] CARRUBA V, NESVORNY D, VOKROUHLICKY D, et al. Detection of the YORP effect for small asteroids in the KARIN cluster[J]. The Astronomical Journal, 2016. DOI: http://10.3847/0004-6256/151/6/164.

[2] CASTILLO-ROGEZ J C, PAVONE M, NESNAS I, et al. Expected science return of spatially-extended in-situ exploration at small Solar system bodies[C]//Proceedings of Aerospace Conference. [S.l.]: IEEE, 2012.

[3] WEN T G, ZENG X Y, CIRCI C, et al. Hop reachable domain on irregularly shaped asteroids[J]. Journal of Guidance, Control, and Dynamics, 2020. DOI: http://10.2514/1.G004682.

[4] LI Z W, ZENG X Y, WANG S Q. Hopping trajectory planning for asteroid surface exploration accounting for terrain roughness[J]. Transactions of the Japan Society for Aeronautical and Space Sciences, 2021, 64(4): 205-214.

[5] PAVONE M, CASTILLO-ROGEZ J C, NESNAS I A D, et al. Spacecraft/rover hybrids for the exploration of small solar system bodies[C]//Proceedings of 2013 IEEE Aerospace Conference. [S.l.]: IEEE, 2013: 1-11.

[6] GAJAMOHAN M, MERZ M, THOMMEN I, et al.

The Cubli：A cube that can jump up and balance[C]// Proceedings of IEEE/RSJ International Conference on Intelligent Robots & Systems. [S.l.]：IEEE, 2012：3722-3727.

[7] GAJAMOHAN M, MUEHLEBACH M, WIDMER T, et al. The cubli：A reaction wheel based 3D inverted pendulum[C]//Proceedings of Control Conference. [S.l.]：IEEE, 2013.

[8] ROMANISHIN J W, GILPIN K, RUS D. M-blocks：Momentum-driven, magnetic modular robots[C]//Proceedings of IEEE/RSJ International Conference on Intelligent Robots & Systems. [S.l.]：IEEE, 2013.

[9] KOENIG A W, PAVONE M, CASTILLO-ROGEZ J C, et al. A dynamical characterization of internally-actuated microgravity mobility systems[C]//Proceedings of IEEE International Conference on Robotics & Automation. [S.l.]：IEEE, 2014.

[10] HOCKMAN B, FRICK A, NESNAS I, et al. Design, control, and experimentation of internally-actuated rovers for the exploration of low-gravity planetary bodies[M]. [S.l.]：Springer International Publishing, 2016.

[11] WANG F, LI C, NIU S, et al. Design and analysis of a spherical robot with rolling and jumping modes for deep space exploration[J]. Machines, 2022, 10：126.

[12] CHENG L, WANG Z, GONG S. Adaptive control of hypersonic vehicles with unknown dynamics based on dual network architecture[J]. Acta Astronautica, 2022, 193：197-208.

[13] MIAO X, SONG Y, ZHANG Z, et al. Successive convexification for ascent trajectory replanning of a multi-stage launch vehicle experiencing non-fatal dynamic faults[J]. IEEE Transactions on Aerospace and Electronic Systems, 2022. DOI：http://10.1109/TAES.2021.3133310.

Author　Dr. **ZENG Xiangyuan** is an associate professor and Ph.D. supervisor in the School of Automation, Beijing Institute of Technology. He received his Ph.D. degree from Tsinghua University and was a visiting student at Texas A&M University in 2011—2012 with Prof. Kyle T. Alfriend. He was also a visiting professor in the Sapenzia University of Rome in 2018. Currently, he is an AIAA astrodynamics technical committee member. He has also served as an associate editor of the journal Advances in Space Research, and an editorial member of the journal Astrodynamics.

Author contributions　Dr. **ZENG Xiangyuan** proposed the development of a low-gravity testbed, formulated the dynamics of the cubic rover and the low-gravity testbed, and summarized the whole manuscript. Mr. **JIANG Bowen** designed and constructed the low-gravity testbed, developed the course of action for mobility experiments, analyzed the dynamics of the cubic rover, and wrote the section on cubic rover's dynamics and ground experiments. Mr. **HUSSAIN Muhammad Talha** designed and constructed the low-gravity testbed jointly, conducted the mobility experiments, analyzed the experimental data, and wrote the section on low-gravity testbed and its validation. Mr. **JIANG Jianxun** developed the hardware and the software of the cubic rover, and contributed to the background of the study. Mr. **YANG Runyi** contributed to the formulation of low-gravity testbed dynamics and the control of cubic rover. All authors commented on the manuscript draft and approved the submission.

Competing interests　The authors declare no competing interests.

（Production Editor：ZHANG Huangqun）

低重力模拟平台上立方体巡视器姿态控制实验研究

曾祥远[1]，姜博文[1]，HUSSAIN Muhammad Talha[1]，姜建勋[2]，杨润一[1]

（1.北京理工大学自动化学院,北京 100081,中国；2.中国船舶工业系统工程研究院,北京 100094,中国）

摘要：小行星表面探测具有重要科学意义,然而目前内驱动巡视器在小天体表面上的运动没有足够的可控性。为了研究立方体巡视器在地表上的姿态控制特性,利用自行设计的立方体巡视器与低重力模拟平台开展了一系列实验研究。实验集中研究了立方体巡视器在翻滚调姿时的飞轮临界转速与不同重力环境的关系以及巡视器在平面调姿时飞轮转速与调姿角度的关系。首先推导了巡视器翻滚调姿和平面调姿的动力学模型；之后介绍了低重力模拟平台的设计与搭建,包括其动力学模型、结构组成与精度验证；最后针对动力学模型与实验数据进行了对比分析,为立方体巡视器在低重力环境下的姿态控制提供了理论与数据参考。

关键词：立方体巡视器；低重力平台；翻滚调姿；平面调姿；表面探测